Modern Physics Letters B
Vol. 33, No. 0 (2021) 2150202 (19 pages)

DOI: 10.1142/S021798492150202X

Please check title, author names, affiliations and emails.

Please check throughout text for spelling errors, figures and tables

Assessment of bioconvection in magnetized Sutterby nanofluid configured by a rotating disk: A numerical approach

M. Ijaz Khan*, Hassan Waqas†, Umar Farooq†, Sami Ullah Khan‡, Yu-Ming Chu§,¶,** and S. Kadry‖

*Department of Mathematics and Statistics, Riphah International University I-14, Islamabad 44000, Pakistan

†Department of Mathematics, Government College University Faisalabad, Layyah Campus 31200, Pakistan

‡Department of Mathematics, COMSATS University Islamabad, Sahiwal 57000, Pakistan

§Department of Mathematics, Huzhou University, Huzhou 313000, China

¶Hunan Provincial Key Laboratory of Mathematical Modeling and Analysis in Engineering, Changsha University of Science and Technology, Changsha 410114, China

‖Department of Mathematics and Computer Science, Beirut Arab University, Beirut, Lebanon

**chuyuming@zjhu.edu.cn

Received 17 September 2020
Revised 6 November 2020
Accepted 10 November 2020
Published

Owing to the growing interest of bioconvection flow of nanomaterials, many investigations on this topic have been performed, especially in this decade. The bioconvection flow of nanofluid includes some novel significance in era of biotechnology and bio-engineering like bio-fuels, microbial enhanced oil recovery, enzymes, pharmaceutical applications, petroleum engineering, etc. The current analysis aims to explore the various thermal properties of Sutterby nanofluid over rotating and stretchable disks with external consequences of variable thermal conductivity, heat absorption/generation consequences, activation energy and thermal radiation. The considered flow problem is changed into dimensionless form with convenient variables. The numerical structure for the obtained non-dimensional equations is numerically accessed with built-in shooting technique. The consequences of various physical parameters are observed for enhancement of velocity, temperature, concentration and motile microorganism. It is noted that both axial and tangential velocity components decrease with Reynolds number and buoyancy ratio

**Corresponding author.

parameter. The nanofluid concentration improves with activation energy and concentration Biot number. Moreover, an improved microorganisms profile is noticed with microorganism Biot number and bioconvection Rayleigh number.

Keywords: Bioconvection flow; Sutterby nanofluid; rotating disk; numerical scheme.

1. Introduction

The nanomaterials have innovative and progressive thermal characteristics which make these nanoparticles more suitable mechanism of heat and mass transportations. Due to improved thermal features of nanomaterials, the scientists have devoted their time to explore the more diligent aspects of such nanomaterials. These thermally improved nanosized particles enhance the thermal efficiency and the rate of heat transfer as comparison to base fluids. In spite to the diverse applications of nanofluids, the investigators have granted a firm commitment to correct exhausting nanofluids from heat dislocation. The standard fluids such as glycol mixture, ethylene, gas and oil have low levels thermal performances which allow poor transportation of energy in various industries and technologies. The first investigation of nanofluids was directed by Choi[1] which proved that upon interaction of tinny nanoparticles in based liquids, the performances become progressive. Due to small size (1–100 nm), the nanomaterials easily immersed into the base fluid. In order to accelerate the convection of nanoliquid, Buongiorno[2] suggested two major features of nanofluid, namely, thermophoresis and Brownian motion. A note worthy literature on nanofluid applications and thermal properties is continued by researchers. For example, Ellahi *et al.*[3] investigated the role of slippage in two-phase flow of nanofluid. Hayat *et al.*[4] investigated the two-dimensional (2D) nanofluid flow with applications of Darcy–Forchheimer law over a bent stretching surface. Khan and Shehzad[5] presented accelerated configuration flow Carreau nanofluid analytically. Ibrahim and Shankar[6] studied the movement and heat transfer of nanofluid over porous stretching surfaces with impact of electromagnetic, thermal radiation and slipping boundary conditions. Turkyilmazoglu[7] inspected the nanoliquid flow in an asymmetric tube by following Buongiorno nanofluid model. Hsiao[8] discussed radiative flow of Carreau nanofluid using a variable control system. In the case of heat absorption/generation, Raju *et al.*[9] concentrated on maximizing convection using nanofluid. Sivasankaran *et al.*[10] observed the natural convection flow of nanofluid over porous directed cavity. Ahmad *et al.*[11] addressed the unsteady 3D flow of the second grade nanofluid owing to applications of thermophoresis and Brownian motion features. Irfan *et al.*[12] reported the dual solution existence of the incompressible fluid of Carreau magnetite nanofluids problem due to shrinkage/stretching configuration with dynamic influence of heat flux, viscous dissipation, Joule heating and heat source/sink. Hsiao[13] examined the micropolar nanofluid flow confined by stretched surface in additional feature of viscous dissipation. Hashim *et al.*[14] presented an innovative analysis to perform mathematical simulations for non-Newtonian Williamson liquid with nanoparticles and nonlinear radiation impact.

Hsiao[15] reported the slip mechanism in convective flow of magnetized nanofluid under the additional impact of electrical field. In another nanofluid analysis, Hsiao[16] claimed some interesting applications of Maxwell nanomaterials in extrusion processes and thermal engineering. Hayat *et al.*[17] inspected the properties of chemical reactive Sutterby nanofluid over a rotating disk.

Bioconvection phenomenon occurs when the self-propelled gyrotactic motile microorganisms upgrade the ordinary fluid density in a particular direction where motile microorganisms swim upwardly in the ordinary fluid due to density gradient. In such situation, an unstable density distribution exists because of the gathering of microorganisms; the top surface of the suspensions becomes too dense causes the microorganisms to fall. The bioconvection pattern is maintained by return up swimming of microorganisms. The tiny organisms that can be seen only by using a microscope are known as microorganisms. Due to the upward swimming phenomenon, it involves gyrotactic motile microorganisms like algae. The motile microorganisms tend to concentrate in the upper part of the fluid which result in unstable density stratification. The swimming patterns of motile microorganisms are premeditated in fluid and other denser substances due to their major presence in fuel cells, pesticides, ethanol and organic fuels. The study of bioconvection in nanofluid is associated with the density strati?cation and the spontaneous pattern formation induced by a collaboration of the denser self-propelled gyrotactic motile microorganisms, buoyancy forces and nanoparticles. The combination of gyrotactic motile microorganisms and nanofluids upturns its stability as a suspension. Kuznetsov[18] put forward to examine the bioconvection flow of nanofluid. Zhang *et al.*[19] reported the results for oxytactic microorganisms and shall be transferred-bioconvection nanofluid flow bundled in a white Riga plate. Bhatti *et al.*[20] examined the swimming of motile microorganisms and nanomaterials in the blood flow via anisotropic tapered arteries. Shahid *et al.*[21] followed a mathematical approach for swimming of gyrotactic microorganisms in nanoparticles over a permeable substrate over a stretching sheet. Ayodeji *et al.*[22] investigated the thermophoresis, viscous dissipation and Brownian motion effects in MHD bioconvection flow of nanofluid with additional features of slip over a stretching layer. Khan *et al.*[23] examined bioconvection in two stretchable moving disks with entropy replication of the Buongiorno nanofluid process. Li *et al.*[24] investigated the bioconvection flow of generalized second-grade nanofluid in presence of Wu's slippage. Muhammad *et al.*[25] studied the influence of bioconvection in Carreau nanofluid flow over a moving wedge. Amirsom *et al.*[26] investigated the flow of non-Newtonian nanofluid with swimming motile microorganisms through a needle with Stefan blowing. Uddin *et al.*[27] examined multiple slip and Stefan blowing features in bioconvection flow of nanofluid numerically. Rashad *et al.*[28] explored the bio-convective flow of nanofluid along with motile microorganisms around a circular cylinder. Ali *et al.*[28] employed the finite element approach to analyze the bioconvection assessment in nanofluid over a vertically stretched surface. The bio-convective flow of nanofluid induced by a paraboloid revolution surface with magnetic force effects has been numerically intended by Khan *et al.*[30] Hosseinzadeh *et al.*[31] analyzed the motile microorganism's applications in 3D cross nanofluid flow numerically.

This numerical investigation deals with the bioconvection flow of Sutterby nanofluid over a rotating disk in presence of heat absorption and generation features. The motivations of current analysis are summarized as follows:

- Examine the thermal performance of Sutterby nanofluid immersed in viscous fluid in presence of different thermal features.
- The flow has been induced by a rotating and stretchable disk.
- The thermal conductivity of Sutterby nanofluid is assumed to be variable.
- The impact of magnetic force, heat absorption/generation, chemical reaction and thermal radiation are also taken into account.
- The modeled problem yield complicated nonlinear differential equations for the flow problem which are numerical tacked by using BVP4C algorithm.
- The improvement in heat and mass transportation is analyzed for different parameters with help of various graphs.

2. Mathematical Formulation

The thermal assessment of Sutterby nanofluid due to the rotating stretching disk is analyzed in this contribution. In addition, the chemical reactions, magnetic field and motile microorganisms are also taken into account. The disk is oriented at $z = 0$ and fluid occupy field $z > 0$ (see Fig. 1). The rotation of disk is taken place along z-axis while it stretched along radial direction. At the disk surface, the nanofluid temperature, concentration and motile microorganisms are reflected by T_w, C_w and N_w, respectively. The far stream nanofluid thermal, concentration and motile microorganisms are denoted by T_∞, C_∞ and N_∞, respectively. Mathematical terminology for governing problem is given as[17]

$$\partial_r u + \partial_z w + u/r = 0, \tag{1}$$

$$\rho(u\partial_r u + w\partial_z u - \nu^2/r) = \mu\partial^2_{zz}u - \delta B_0^2 u + \frac{1}{\rho_f}\begin{bmatrix}(1-C_f)\rho_f\beta^{**}g*(T-T_\infty) - (\rho_p-\rho_f)g^*(C-C_\infty)\\ -(N-N_\infty)g^*\gamma(\rho_m-\rho_f)\end{bmatrix}, \tag{2}$$

$$\rho(u\partial_r u + w\partial_z u - uv^2/r) = \mu\partial^2_{zz}v - \delta B_0^2 v, \tag{3}$$

$$u\partial_r T + w\partial_z T = \frac{1}{(\rho c)_f}\partial_z(K(T)\partial_z T) + (k*/(\rho c)_f)(\partial^2_{zz}T) + (Q_0/(\rho c)_f)(T-T_\infty) + \tau[D_B(\partial_z C)(\partial_z T) + (D_T/T_\infty)(\partial_z T)^2] + \partial_z\left(\frac{16\sigma^* T^3}{3k^*(\rho c)_f}\partial_z T\right), \tag{4}$$

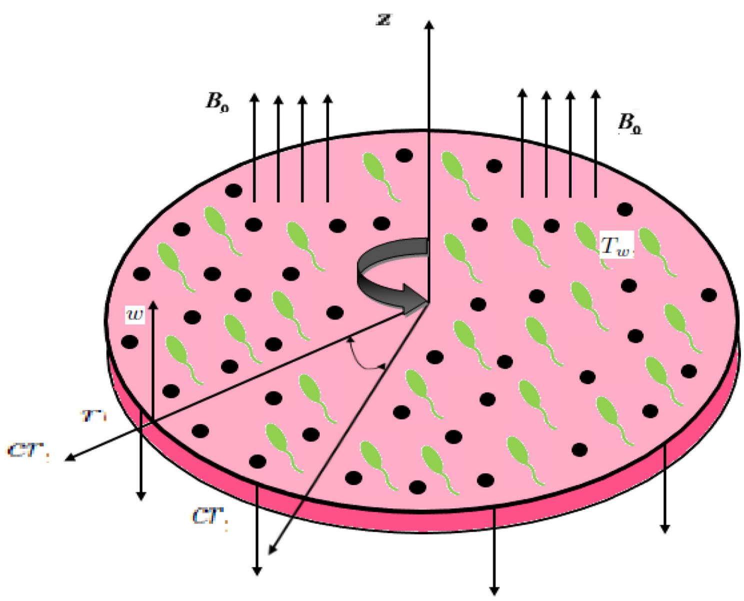

Fig. 1. (Color online) Geometry of problem.

$$u\partial_r C + w\partial_z C = \frac{1}{(\rho c)_f}\partial_z(D(C)\partial_z C) + D_B\partial^2_{zz}C + (D_T/T_\infty)(\partial^2_{zz}T) - k_r^2(C - C_\infty)\left(\frac{T}{T_\infty}\right)^m \exp\left(\frac{-E_a}{KT}\right), \tag{5}$$

$$u\partial_r N + v\partial_z N + [(\partial_z N)(\partial^2_{zz}C)](bW_c/(C_w - C_\infty)) = D_B(\partial^2_{zz}N). \tag{6}$$

The appropriate form of boundary conditions is articulated as follows[17]:

$$\left.\begin{aligned} &u(0) = cr, v(0) = \varpi r, w(0) = 0, -k\partial_z T = h_T(T_w - T),\\ &-D_B\partial_z C = h_C(C_w - C), -D_B\partial_z N = h_m(N_w - N),\\ &u(\infty) \to 0, \nu(\infty) \to 0, T(\infty) \to T_\infty, C(\infty) \to C_\infty, N(\infty) \to N_\infty \end{aligned}\right\}. \tag{7}$$

Here (u, v, w) stand for velocity components, (μ) stand for dynamic viscosity, density (ρ, δ) electric conductivity, (N) motile microorganisms, (T) temperature, (τ) heat capacities ratio, (T_∞) ambient temperature, (cp) specific heat, (D_T) coefficient of thermophoresis diffusion, (D_B) coefficient of Brownian diffusion, strength of applied magnetic field (B_0), (C) stand for concentration, (k_r^2) stand for chemical reaction rate constant, (E_a) the coefficient of activation energy, (β^{**}) for volume expansion coefficient, (g^*) stand for density, σ^* for Stefan–Boltzmann constant, (Q_0) heat absorption generation coefficient and $(k*)$ is signifies Boltzmann constant.

In Sutterby fluid model conditions, the viscosity relationship is preferred as

$$\mu = \mu_0[\sin h^{-1}(B\Delta)/B\Delta]^m, \tag{8}$$

where (μ_0, m, B) stand for positive parameters and (Δ) stand for the shear rate. Moreover, (B) symbolize the characteristic time parameter, (μ_0) denotes the viscosity at low and high shear rates, (m) stand for dimensionless quantity. It is remarked that when $(m = 0)$, Sutterby model forecast the viscous fluid nature while $(m = 1)$ diminishes the Eyring model.

By binomial contraction, one can remember as follows:

$$\mu \cong \mu_0[1 - (B\Delta)^2/6]^m \cong \mu_0[1 - m(B\Delta)^2/6]. \tag{9}$$

Now shear rate Δ can be defined as

$$\Delta = \sqrt{\frac{1}{2}\mathrm{trace}(\Delta_1^2)}. \tag{10}$$

The thermal conductivity and mass diffusivity are simplified as

$$K(T) = k_\infty\left[1+\in_1\left(\frac{T - T_\infty}{\Delta T}\right)\right], \quad D(C) = k_\infty\left[1+\in_2\left(\frac{C - C_\infty}{\Delta C}\right)\right].$$

The first-order Rivlin–Erickson tensor is described by $\Delta_1 = L + L^T$. The dimensionless variables are[17]

$$\left.\begin{array}{l} u = rwf'(\zeta), v = rwg'(\zeta), w = 2iwf(\zeta), \theta(\zeta) = (T - T_\infty/T_w - T_\infty), \\ \varphi(\zeta) = (C - C_\infty/C_w - C_\infty), \chi(\zeta) = (N - N_\infty/N_w - N_\infty), \zeta = z/i \end{array}\right\}. \tag{11}$$

Introducing the above transformation in governing equations yields:

$$f''' - 2n\varepsilon^2[2f'f''^2 + f'^2f'''] + \mathrm{Re}[g^2 + 2f'f'' - f'^2] - M\mathrm{Re}f' + \lambda(\theta - \mathrm{Nr}\phi - \mathrm{Nc}\chi) = 0, \tag{12}$$

$$g'' - 2n\varepsilon^2[2f'f''^2g' + f'^2g''] + 2\mathrm{Re}[f'g - f'g'] - M\mathrm{Re}g' = 0, \tag{13}$$

$$(1+\in_1\theta)\theta''+\in_1\theta'^2 + \mathrm{Nb}\,\mathrm{Pr}\,\theta'\phi' + \mathrm{Pr}\,\mathrm{Nt}\theta'^2 + \beta\,\mathrm{Pr}\,\theta + 2\mathrm{Re}\,\mathrm{Pr}\,f\theta' + \mathrm{Rd}(3(1 + \theta(\theta_w - 1))^2(\theta_w - 1)\theta'^2 + (1 + \theta(\theta_w - 1))^3\theta'') = 0, \tag{14}$$

$$(1+\in_2\phi)\phi''+\in_2\phi'^2 + 2\mathrm{ReSc}f\phi' + \frac{\mathrm{Nt}}{\mathrm{Nb}}\theta'' - \mathrm{Sc}K_1(1 + \omega\theta)^m\exp\left(\frac{-E}{1 + \omega\theta}\right)\phi = 0, \tag{15}$$

$$\chi'' + 2\mathrm{ReLb}f\chi' - \mathrm{Pe}[\phi''(\chi + \delta_1) + \chi'\phi'] = 0, \tag{16}$$

$$\left.\begin{array}{l} f(0) = 0, f'(0) = A, \\ f'(\infty) \to 0, g(0) = 1, g(\infty) \to 0, \\ \theta'(0) = -\gamma_1(1 - \theta(0)), \phi'(0) = -\gamma_2(1 - \phi(0)), \\ \chi'(0) = -\gamma_3(1 - \chi(0)), \\ \theta(\infty) \to 0, \phi(\infty) \to 0, \chi(\infty) \to 0, \end{array}\right\} \tag{17}$$

where $\mathrm{Re}(=\omega i^2/\nu)$, signifies Reynolds number, $\varepsilon(=\omega B)$, material parameter, $M(=\delta B_0^2/\rho\omega)$, is magnetic parameter, mixed convection parameter is $\lambda = \frac{(1-C_f)(T_w-T_\infty)\beta^{**}g^*}{rw^2}$ and buoyancy ratio parameter $\mathrm{Nr} = \frac{(\rho_p-\rho_f)(C_w-C_\infty)}{\rho_f\beta^{**}(1-C_f)(T_w-T_\infty)}$, bioconvection Rayleigh number is $\mathrm{Nc} = \frac{(\rho_m-\rho_f)(N_w-N_\infty)\gamma^*}{\rho_f\beta^{**}(1-C_f)(T_w-T_\infty)}$, Prandtl number $\mathrm{Pr}(=(\rho c_p)_f\nu/k)$, Schmidt number $\mathrm{Sc}(=\nu/D_B)$, ratio of stretching parameter $A(=c/\omega), K_1(=K_r^2/\nu)$, the chemical reaction parameter, radiation parameter is $\mathrm{Rd} = \frac{16\sigma^* T_\infty^3}{3k^* k_f}$, $\theta_w = \frac{T_w}{T_\infty}$ be the temperature ratio parameter, $\mathrm{Nb}(=\tau D_B(C_w-C_\infty)/\nu)$ Brownian parameter and $\mathrm{Nt}(=\tau D_T(T_w-T_\infty)/\nu T_\infty)$, thermophoresis parameter, temperature difference parameter and activation energy parameter are $\omega = \frac{T_\infty}{(T_w-T_\infty)}, E = \frac{E_a}{K(T_w-T_\infty)}$, heat source parameter to angular velocity $\beta(=Q_0h^2/(\rho c_p)_f\nu)$, bioconvection Lewis number is $\mathrm{Lb}(=\nu/D_m)$ and Peclet number is $\mathrm{Pe}(=bW_c/D_m), \gamma_1 = \frac{h_T}{k}\sqrt{\frac{i}{z}}$ the thermal Biot number, $\gamma_2 = \frac{h_C}{D_B}\sqrt{\frac{i}{z}}$ for concentration Biot number and $\gamma_3 = \frac{h_m}{D_m}\sqrt{\frac{i}{z}}$ the microorganism Biot number.

Now the dimensionless forms of surface drag force, local Nusselt number, local Sherwood number and motile density number are defined via the following relations[17]:

$$\left.\begin{aligned} &C_{f_r} = (-2/(\mathrm{Re}_r)A^2)(1-2n\varepsilon^2(f'(0)^2))f''(0),\\ &C_{f_\theta} = (-2/(\mathrm{Re}_r))(1-2n\varepsilon^2(f'(0)^2))g'(0),\\ &\mathrm{Nu}_r = -\theta'(0), \mathrm{Sh}_r = -\phi'(0). \end{aligned}\right\} \tag{18}$$

where $\mathrm{Re}_r = \mathrm{r}i\omega/\nu$ indicates the local Reynolds number.

3. Numerical Scheme

It is observed that Eqs. (10)–(14) with boundary condition (15) represent the nonlinear system for which computation of numerical solution is a task. On this end, famous shooting technique is used to formulate the controlling equations. Before starting the procedure, higher order equations are entrenched into first-order scheme as follows:

$$\left.\begin{aligned} &f = q_1, f' = q_2, f'' = q_3, f''' = q_3', g = q_4, g' = q_5, g'' = q_5',\\ &\theta = q_6, \theta' = q_7, \theta'' = q_7'\phi = q_8, \phi' = q_9, \phi'' = q_9',\\ &\chi = q_{10}, \chi' = q_{11}, \chi'' = q_{11}', \end{aligned}\right\} \tag{19}$$

$$q_3' = \frac{4n\varepsilon^2 q_2 q_3^2 - \mathrm{Re}[q_4^2 + 2q_2q_3 - q_2^2] + M\mathrm{Re}q_2 - \lambda(q_6 - \mathrm{Nr}q_8 - \mathrm{Nc}q_{10})}{1-2n\varepsilon^2 q_2^2}, \tag{20}$$

$$q_5' = \frac{4n\varepsilon^2 q_2 q_3^2 q_5 - 2\mathrm{Re}[q_2q_4 - q_2q_5] + M\mathrm{Re}q_5}{1-2n\varepsilon^2 q_2^2}, \tag{21}$$

$$q_7' = \frac{-\in_1 q_7^2 - \mathrm{Nb}\,\mathrm{Pr}\,q_7 q_9 - \mathrm{Pr}\,\mathrm{Nt} q_7^2 - \beta\,\mathrm{Pr}\,q_6 - 2\mathrm{Re}\,\mathrm{Pr}\,q_1 q_7 + \mathrm{Rd}(3(1+q_6(\theta_w-1))^2(\theta_w-1)q_7^2)}{(1+\in_1 q_6) + \mathrm{Rd}((1+q_6(\theta_w-1))^3)}, \tag{22}$$

$$q_9' = \frac{-\in_2 q_9^2 - 2\mathrm{ReSc} q_1 q_9 - \frac{\mathrm{Nt}}{\mathrm{Nb}} q_7' + \mathrm{Sc} K_1 (1+\omega q_6)^m \exp\left(\frac{-E}{1+\omega q_6}\right) q_8}{(1+\in_2 q_8)}, \tag{23}$$

$$q_{11}' = -2\mathrm{Lb} q_{11} q_1 + \mathrm{Pe}[q_9'(q_{10}+\delta_1) + q_{11} q_9], \tag{24}$$

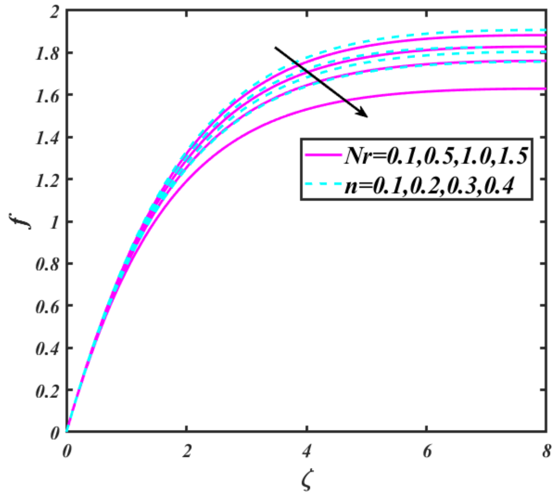

Fig. 2. (Color online) Significance of Nr and n over f.

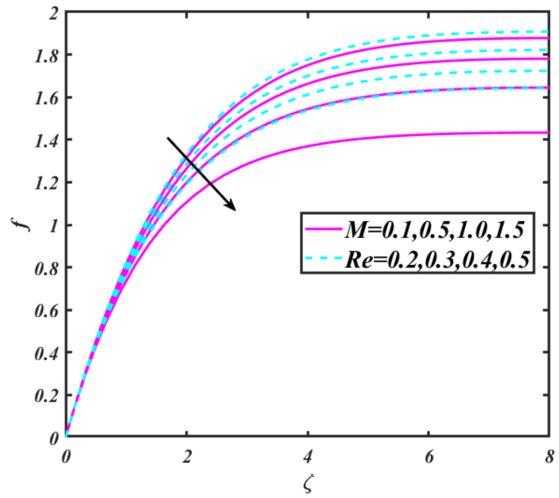

Fig. 3. (Color online) Significance of M and Re over f.

1 with

$$\left.\begin{array}{l} q_1(0)=0, q_2(0)=A, \\ \quad q_2(\infty)\to 0, q_4(0)=1, q_4(\infty)\to 0, \\ \quad q_7(0)=-\gamma_1(1-q_6(0)), q_9(0)=-\gamma_2(1-q_8(0)), \\ \quad q_{11}(0)=-\gamma_3(1-q_{10}(0)), \\ \quad q_6(\infty)\to 0, q_8(\infty)\to 0, q_9(\infty)\to 0. \end{array}\right\} \quad (25)$$

2

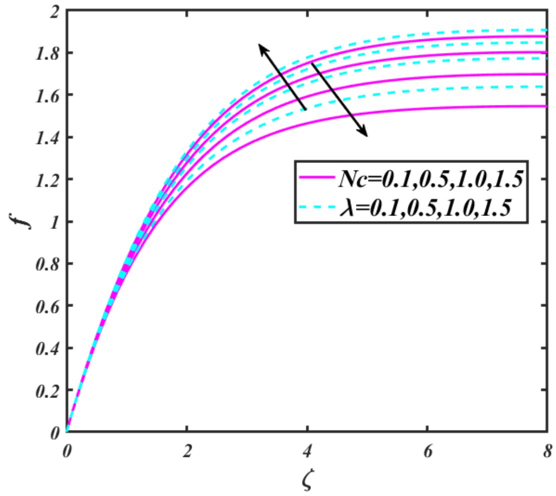

Fig. 4. (Color online) Significance of NC and λ over f.

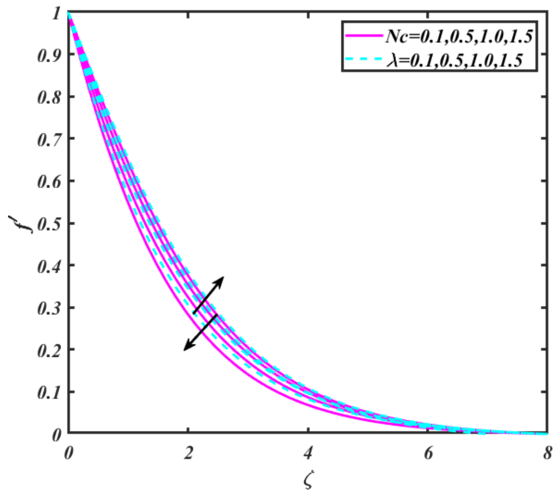

Fig. 5. (Color online) Significance of NC and λ over f'.

4. Discussion

Present segment consists of inclusive discussion about the physical behavior of numerous parameters. Figure 2 delineates the influence of buoyancy ratio parameter Nr and dimensionless constant n on the axial velocity profile f. From this curve, we scrutinize that the f collapsed by the intensification of the bouncy ratio parameter and dimensionless constant. The upshot of magnetic parameter M and Reynolds number Re on the axial velocity f is evaluated in Fig. 3. It utilized that axial velocity of the liquid decays with growing valuation of magnetic parameter

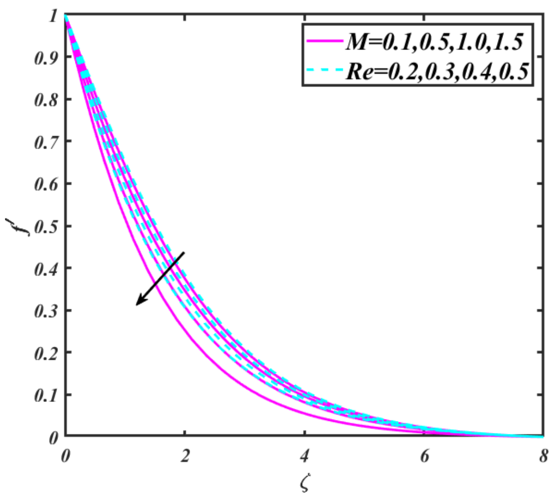

Fig. 6. (Color online) Significance of M and Re over f'.

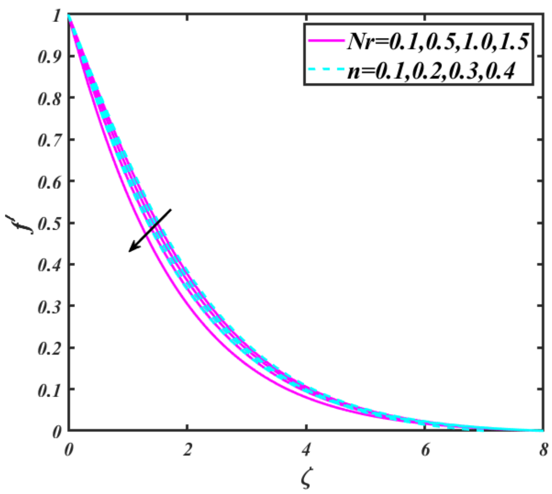

Fig. 7. (Color online) Significance of Nr and n over f'.

and Reynolds number. The outcomes of bioconvection Rayleigh number Nc and mixed convection parameter λ against axial velocity profiles f are demonstrated in Fig. 4. It can be perceived that axial velocity of fluid is condensed with enlarged values of bioconvection Nc and λ. The behavior of bioconvection Rayleigh number Nc and mixed convection parameter λ against radial velocity profiles f' is illustrated in Fig. 5. It is sighted that the radial velocity of liquid is enhanced for higher valuation of mixed convection parameter while it fall down by swelling of

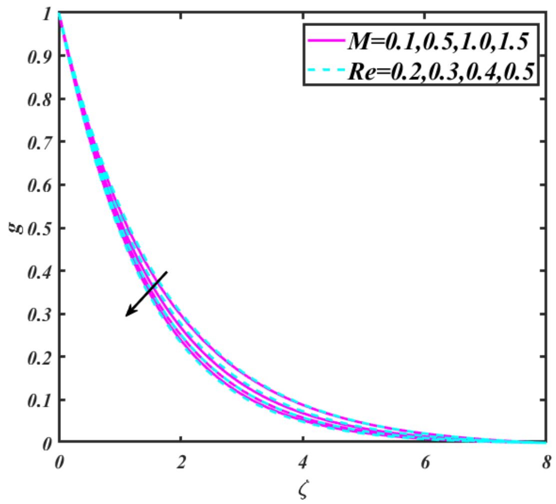

Fig. 8. (Color online) Significance of M and Re over g.

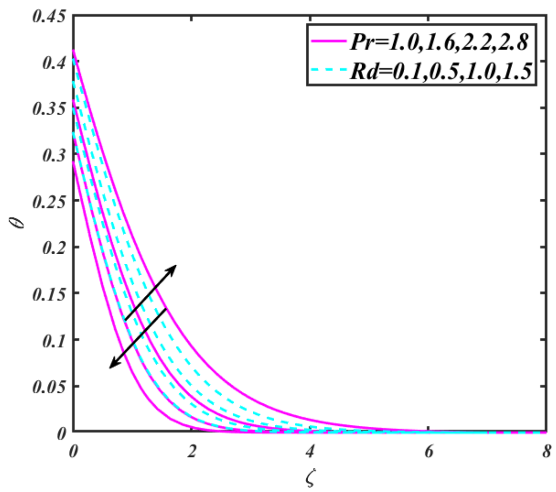

Fig. 9. (Color online) Significance of Pr and Rd over θ.

bioconvection Rayleigh number. Figure 6 discloses the significant features of magnetic parameter M and Reynolds number Re on the radial velocity f'. From the curve, it is noticed that radial velocity decreases for leading variation of magnetic parameter M and Reynolds number. Figure 7 depicts the features of buoyancy ratio parameter Nr and dimensionless constant n on the radial velocity profile f'. It is explored that the arising values of buoyancy ratio parameter Nr and dimensionless constant diminishes the velocity concentration. Figure 8 is structured to estimate the effects of magnetic parameter M and Reynolds number Re on the azimuthal

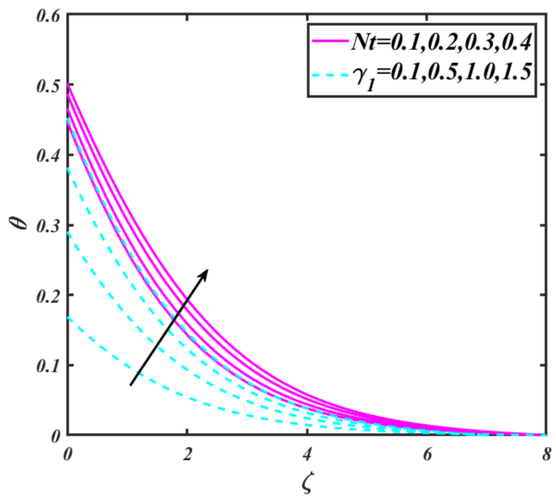

Fig. 10. (Color online) Significance of Nt and γ_1 over θ.

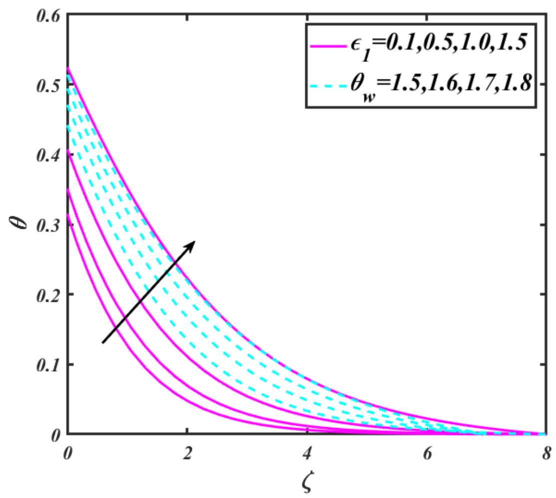

Fig. 11. (Color online) Significance of ε_1 and θ_w over θ.

velocity component g. It is suggested that the azimuthal velocity declined for magnetic parameter M and Reynolds number Re. The importance of radiation parameter Rd and Prandtl number Pr on the concentration of nanoparticles ϕ is shown in Fig. 9. A fall in θ is noted with leading change in Prandtl number while temperature upsurge by increasing radiation parameter Rd. Figure 10 identifies the effect of thermophoresis constant Nt and thermal Biot number γ_1 on temperature profile θ. This figure conveyed that temperature profile is enhanced with escalating values of thermophoresis parameter and thermal Biot number. The impacts of material parameter ε_1 and temperature ratio parameter θ_w on θ is demonstrated in

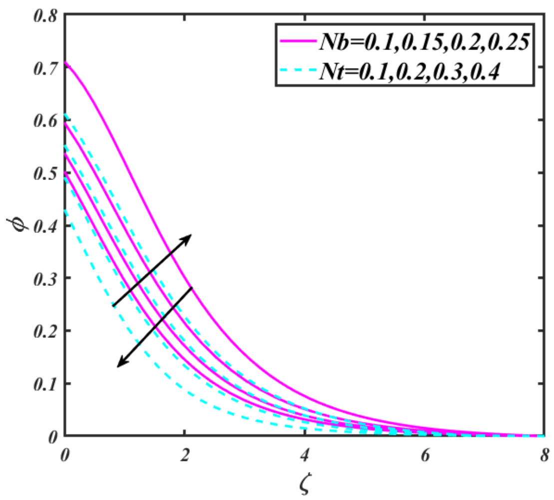

Fig. 12. (Color online) Significance of Nb and Nt over ϕ.

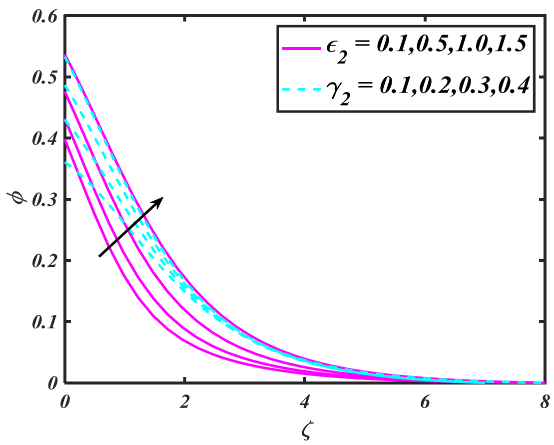

Fig. 13. (Color online) Significance of ε_2 and γ_2 over ϕ.

Fig. 11. It is observed that for growing values of material parameter and temperature ratio parameter, a boosted temperature of fluid is observed. Figure 12 aims to evaluate the characteristics of ϕ for thermophoresis variable Nt and Brownian motion parameter Nb. The concentration profile decays for higher numerical values of Brownian motion parameter Nb while an increasing behavior of ϕ has been noticed with Nt. The consequences of γ_2 and ε_2 on ϕ are found in Fig. 13. The mounting valuation in concentration field ϕ is examined by the increasing attitude γ_2 and ε_2. In Fig. 14, the variation of Schmidt number Sc and activation energy E

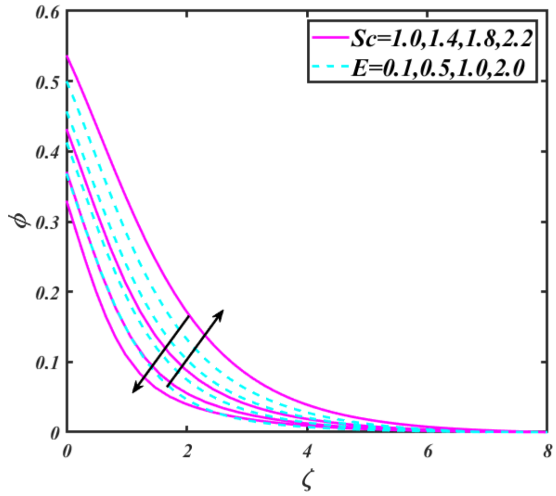

Fig. 14. (Color online) Significance of Sc and E over ϕ.

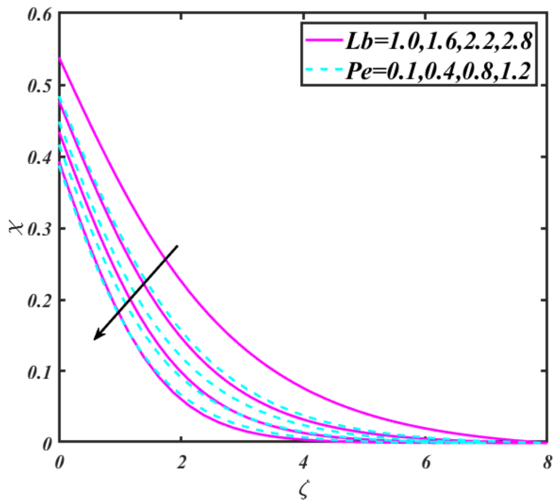

Fig. 15. (Color online) Significance of Lb and Pe over χ.

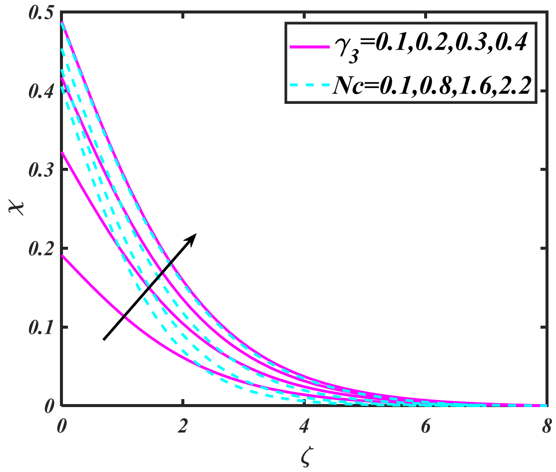

Fig. 16. (Color online) Significance of γ_3 and Nc over χ.

Table 1. Outcomes of $-f''(0)$ and $-g'(0)$ when Re $= 0.1$, $\varepsilon = 0.2$, Pr $= 0.7$, Sc $= 0.1$, $A = 0.5$, $K_1 = 0.1$, Rd $= 0.4$, $\theta_w = 0.4$, Nb $= 0.4$, Nt $= 0.5$, $\omega = 0.5$, $E = 0.5$, $\beta = 0.5$, Lb $= 0.4$, Pe $= 0.5$, $\gamma_1 = 0.2$, $\gamma_2 = 0.2$, $\gamma_3 = 0.3$.

M	Nr	Nc	λ	$-f''(0)$	$-g'(0)$
0.1	0.2	0.1	0.1	1.4284	0.9385
0.8				1.6854	0.4133
1.6				1.9612	0.3111
0.5	0.1	0.1	0.1	1.3664	0.9412
	1.0			1.4070	0.9394
	2.0			0.4500	0.9375
0.5	0.2	0.2	0.1	1.3595	0.9418
		0.8		1.4052	0.9396
		1.6		1.4518	0.9373
0.5	0.2	0.1	0.2	1.4138	0.9385
			0.8	1.4221	0.9429
			1.6	1.4356	0.9507

on ϕ is observed. The boosting values of Sc fail in the concentration while change in activation energy enlarges the concentration profile ϕ.

The behavior of Lb and Peclet number on motile microorganism distribution χ is designed in Fig. 15. The motile microorganism profile χ is depressed with growing valuation of Lb and Pe. Figure 16 captured consequences of microorganisms Biot number γ_3 and bioconvection Rayleigh number Nc on χ. Here the microorganisms field χ boosted up by enlarging the values of microorganisms Biot number γ_3 and bioconvection Rayleigh number Nc.

Table 2. Outcomes of $-\theta'(0)$ for flow parameters when $\mathrm{Re} = 0.1$, $\varepsilon = 0.2$, $\mathrm{Sc} = 0.1$, $A = 0.5$, $K_1 = 0.1$, $\mathrm{Rd} = 0.4$, $\theta_w = 0.4$, $\omega = 0.5$, $E = 0.5$, $\beta = 0.5$, $\mathrm{Lb} = 0.4$, $\mathrm{Pe} = 0.5$, $\gamma_1 = 0.2$, $\gamma_2 = 0.2$, $\gamma_3 = 0.3$.

M	Nr	Nc	λ	Nt	Nb	Pr	Re	γ	$-\theta'(0)$
0.2	0.2	0.1	0.1	0.5	0.5	1.5	0.8	0.3	0.2632
0.8									0.2634
1.6								0.2639	
0.5	0.2	0.1	0.1	0.5	0.5	1.5	0.8	0.3	0.2630
	0.4								0.2632
	0.6								0.2636
0.5	0.2	0.2	0.1	0.5	0.5	1.5	0.8	0.3	0.2632
		0.4							0.2632
		0.6							0.2636
0.5	0.2	0.1	0.2	0.5	0.5	1.5	0.8	0.3	0.2636
			0.8						0.2640
			1.6						0.2643
0.5	0.2	0.1	0.1	0.1	0.5	1.5	0.8	0.3	0.5615
				0.6					0.5296
				1.2					0.5075
0.5	0.2	0.1	0.1	0.5	0.1	1.5	0.8	0.3	0.5480
					0.6				0.5319
					1.2				0.5179
0.5	0.2	0.1	0.1	0.5	0.5	1	0.8	0.3	0.4403
						2			0.6023
						3			0.7065
0.5	0.2	0.1	0.1	0.5	0.5	1.5	0.1	0.3	0.5767
							0.6		0.5841
							1.2		0.5885
0.5	0.2	0.1	0.1	0.3	0.2	1.5	0.8	0.1	0.0888
								0.6	0.3352
								1.0	0.4274

Table 3. Result of $-\phi'(0)$ when $\mathrm{Re} = 0.1$, $\varepsilon = 0.2$, $A = 0.5$, $K_1 = 0.1$, $\mathrm{Rd} = 0.4$, $\theta_w = 0.4$, $\omega = 0.5$, $E = 0.5$, $\beta = 0.5$, $\mathrm{Lb} = 0.4$, $\mathrm{Pe} = 0.5$, $\gamma_1 = 0.2$, $\gamma_2 = 0.2$, $\gamma_3 = 0.3$.

M	Nr	Nc	Pr	Nb	Nt	λ	Sc	γ	B	$-\phi'(0)$
0.2	0.1	0.1	1.5	0.5	0.5	0.2	0.2	0.3	0.2	0.2355
0.8										0.2405
1.6										0.2473
0.5	0.2	0.1	1.5	0.5	0.5	0.2	0.2	0.3	0.2	0.2363
	0.4									0.2358
	0.6									0.2355
0.5	0.1	0.2	1.5	0.5	0.5	0.2	0.2	0.3	0.2	0.2366
		0.4								0.2359
		0.6								0.2351
0.5	0.1	0.1	1	0.5	0.5	0.2	0.2	0.3	0.2	0.1838
			2							0.1879
			3							0.1938
			1.5	0.2	0.5	0.2	0.2	0.3	0.2	0.0171

Table 3. (*Continued*)

M	Nr	Nc	Pr	Nb	Nt	λ	Sc	γ	B	$-\phi'(0)$
				0.6						0.2036
				1.0						0.2400
0.5	0.1	0.1	1.5	0.5	0.2	0.2	0.2	0.3	0.2	0.2660
					0.6					0.1669
					1.0					0.0994
0.5	0.1	0.1	1.5	0.5	0.5	1.0	1.0	0.3	0.2	0.0951
						1.6	1.6			0.1519
						2.2	2.2			0.1957
0.5	0.1	0.1	1.5	0.5	0.5	0.2	0.2	0.1	0.2	0.2664
								0.6		0.2198
								1.0		0.2035
0.5	0.1	0.1	1.5	0.5	0.5	0.2	0.2	0.3	0.1	0.0607
									0.5	0.2298
									1	0.3527

Table 4. Variation of $-\chi'(0)$ when Re $= 0.1$, $\varepsilon = 0.2$, Pr $= 0.7$, Sc $= 0.1$, $A = 0.5$, $K_1 = 0.1$, Rd $= 0.4$, $\theta_w = 0.4$, Nb $= 0.4$, Nt $= 0.5$, $\omega = 0.5$, $E = 0.5$, $\beta = 0.5$, $\gamma_1 = 0.2$, $\gamma_2 = 0.2$, $\gamma_3 = 0.3$.

M	Nr	Nc	λ	Lb	Pe	$-\chi'(0)$
0.1	0.2	0.1	0.1	1	0.3	0.9385
0.8						0.4133
1.6						0.3111
0.5	0.1	0.1	0.1	1	0.3	0.9412
	1.0					0.9394
	2.0					0.9375
0.5	0.2	0.2	0.1	1	0.3	0.9418
		0.8				0.9396
		1.6				0.9373
0.5	0.2	0.1	0.2	1	0.3	0.9385
			0.8			0.9429
			1.6			0.9507
0.5		0.1		1.2	0.3	0.2499
				1.8		0.2775
				2.6		0.2908
0.5		0.1		1	0.2	0.2422
					0.8	0.2403
					1.6	0.2804

The outcomes of $-f''(0)$ and $-g'(0)$ against various values of M, Nr, Nc and λ are presented in Table 1. An increasing change in $-f''(0)$ is observed for M, Nr, Nc and λ. However, the $-g'(0)$ decreases for these flow parameters. Table 2 aims to report the outcomes of $-\theta'(0)$ against M, Nr, Nc, Nt, Nb, Pr, Rd and λ and γ. The observations reveal that $-\theta'(0)$ decreases for Nt and Nb. Table 3 results variation of $-\phi'(0)$ for against different flow parameters which claim an increasing change in $-\phi'(0)$ due to B, Sc and γ. In Table 4, the numerical variation of $-\chi'(0)$ has been discussed for increasing values of M, Nt, Nb, Lb, λ and Pe. A leading numerical variation is noted for Lb, λ and Pe while other parameters show reverse trend.

5. Conclusions

Existing contact is consistent with the Sutterby nanofluid wave, arising from the release of energy and motile microorganisms on a rotating disk. The eminent shooting scheme is used to crack the flow problems.

- Diminution in velocity profile of Sutterby nanofluid is monitored for increasing valuation of bioconvection Rayleigh number and buoyancy ratio parameter.
- Temperature ratio parameter and thermophoresis parameter boosted the thermal field.
- Higher variation of Prandtl number reduces the thermal profile of Sutterby nanofluids.
- The mounting valuation of activation energy parameter enhanced the solutal field of Sutterby fluid model with bioconvection and solutal field reduced by Brownian motion parameter.
- The growing values of bioconvection Lewis number and Peclet number cause reduction in microorganism field.
- These results for flow of non-Newtonian nanomaterials include applications in cooling processes, nuclear reactor, microelectronics, energy production, transformer oil, thermal extrusion processes, etc.

Acknowledgments

The research was supported by the National Natural Science Foundation of China (Grant Nos. 11971142, 11871202, 61673169, 11701176, 11626101 and 11601485).

References

1. S. U. S. Choi, Enhancing thermal conductivity of fluids with nanoparticles, in *Developments and Applications of Non Newtonian Fluids*, Vol. 66, AJME, FED 231/MD (1995), p. 99105.
2. J. Buongiorno, *J. Heat Transf.* **128** (2006) 240.
3. R. Ellahi, F. Hussain, S. A. Abbas, M. M. Sarafraz, M. Goodarzi and M. S. Shadloo, *Inventions* **5**(1) (2020) 6.
4. T. Hayat, S. Qayyum, A. Alsaedi and B. Ahmad, *Int. Commun. Heat Mass Transf.* **111** (2020) 104445.
5. S. U. Khan and S. A. Shehzad, *Adv. Mech. Eng.* **11**(12) (2019) 1.
6. W. Ibrahim and B. Shankar, *Comput. Fluids* **75** (2013) 1.
7. M. Turkyilmazoglu, *Int. J. Heat Mass Transf.* **126** (2018) 974.
8. K. L. Hsiao, *Energy* **130** (2017) 486.
9. C. S. Raju, M. Jayachandrababu, N. Sandeep and P. Mohan Krishna, *Int. J. Eng. Sci.* **6** (2015) 31.
10. S. Sivasankaran, A. I. Alsabery and I. Hashim, *Physica A: Stat. Mech. J.* Pre-proofs and its Applications **509** (2018) 275.

11. M. Ahmad, T. Muhammad, I. Ahmad and S. Aly, *Physica A: Stat. Mech. Appl.* (2020) 124004.
12. M. Irfan, M. Khan, W. A. Khan and L. Ahmad, *Appl. Phys. A* **125** (2019) 179.
13. K.-L. Hsiao, *Int. J. Heat Mass Transf.* **112** (2017) 983.
14. Hashim, M. Khan and A. Hamid, *Eur. Phys. J. Plus* **134** (2019) 50.
15. K.-L. Hsiao, *Appl. Therm. Eng.* **98** (2016) 850.
16. K.-L. Hsiao, *Appl. Therm. Eng.* **112** (2017) 1281.
17. T. Hayat, A. Salman, M. Ijaz Khan and A. Alsaedi, *Commun. Theor. Phys.* **69** (2018) 569.
18. A. V. Kuznetsov, *Int. Commun. Heat Mass Transf.* **32** (2005) 991.
19. L. Zhang, M. M. Bhatti, R. Ellahi and E. E. Michaelides, *J. Non-Equilib. Thermodyn.* (2020), DOI: 10.1142/S021798492150202X10.1515/jnet-2020-0010.
20. M. M. Bhatti, M. Marin, A. Zeeshan, R. Ellahi and S. I. Abdelsalam, *Front. Phys.* (2020), DOI: 10.1142/S021798492150202X10.3389/fphy.2020.00095.
21. A. Shahid, H. Huang, M. M. Bhatti, L. Zhang and R. Ellahi, *Mathematics* **8**(3) (2020) 380.
22. F. Ayodeji, A. Tope and O. Pele, *Mach. Learn. Res.* **4**(4) (2020) 51.
23. N. S. Khan, Q. Shah, A. Bhaumik, P. Kumam, P. Thounthong and I. Amiri, *Sci. Rep.* **10**(1) (2020) 1.
24. Y. Li, H. Waqas, M. Imran, U. Farooq, F. Mallawi and I. Tlili, *Symmetry* **12**(3) (2020) 393.
25. T. Muhammad, S. Z. Alamri, H. Waqas, D. Habib and R. Ellahi, *J. Therm. Anal. Calorim.* (2020) 1.
26. N. A. Amirsom, M. J. Uddin and A. Izani md Ismail, *Heat Transf. Asian Res.* **48**(2) (2019) 727.
27. M. J. Uddin, Y. Alginahi, O. A. Bég and M. N. Kabir, *Comput. Math. Appl.* **72**(10) (2016) 2562.
28. A. M. Rashad and H. A. Nabwey, *J. Taiwan Inst. Chem. Eng.* **99** (2019) 9.
29. B. Ali, S. Hussain, Y. Nie, L. Ali and S. Ul Hassan, *Chin. J. Phys.* **68** (2020) 654.
30. M. Khan, T. Salahuddin, M. Y. Malik, M. S. Alqarni and A. M. Alqahtani, *Physica A: Stat. Mech. Appl.* **553** (2020) 124231.
31. K. Hosseinzadeh, S. Roghani, A. R. Mogharrebi, A. Asadi, M. Waqas and D. D. Ganji, *Alexandria Eng. J.* **59**(5) (2020) 3297.